The use of GPS-arrays in detecting shock-acoustic waves generated during rocket launchings

Afraimovich E. L., Kosogorov E. A., Perevalova N. P.,
and Plotnikov A. V.
Institute of Solar-Terrestrial Physics SD RAS,
p. o. box 4026, Irkutsk, 664033, Russia
fax: +7 3952 462557; e-mail: afra@iszf.irk.ru

Abstract

This paper is concerned with the form and dynamics of shock-acoustic waves (SAW) generated during rocket launchings. We have developed a method for determining SAW parameters (including angular characteristics of the wave vector, and the SAW phase velocity, as well as the direction towards the source) using GPS-arrays whose elements can be chosen out of a large set of GPS-stations of the global GPS network. Contrary to the conventional radio-probing tecniques, the proposed method provides an estimate of SAW parameters without a priori information about the site and time of a rocket launching. The application of the method is illustrated by a case study of ionospheric effects from launchings of launch vehicles (LV) Proton and Space Shuttle from space-launch complexes Baikonur and Kennedy Space Center (KSC) in 1998 and 1999 (a total of five launchings). The study revealed that, in spite of a difference of LV characteristics, the ionospheric response for all launchings had the character of an N–wave corresponding to the form of a shock wave, regardless of the disturbance source (rocket launchings, industrial explosions). The SAW period T is 270–360 s, and the amplitude exceeds the standard deviation of TEC background fluctuations in this range of periods under quiet and moderate geomagnetic conditions by factors of 2 to 5 as a minimum. The angle of elevation of the SAW wave vector varies from 30° to 60° , and the SAW phase velocity (900–1200 m/s) approaches the sound velocity at heights of the ionospheric F-region maximum. The position of the SAW source, inferred by neglecting refraction corrections, corresponds to the segment of the LV Proton path at a distance no less than 700–900 km from the launch pad, and to the LV flying altitude no less than 100 km. For the Space Shuttle LV the position of the SAW source corresponds to the segment of the trajectory

at a distance of at least 200–500 km from the launch pad and to the LV flight altitude of at least 100 km. Our data are consistent with the existing view that SAW are generated during a nearly horizontal flight of the rocket with its engine in operation in the acceleration segment of the path at 100–130 km altitudes in the lower atmosphere.

1 Introduction

A large number of publications, including a variety of thorough reviews (Karlov et al., 1980; Mendillo, 1981; 1982; Nagorsky, 1998; 1999) are devoted to the study of the ionospheric response of the shock wave produced during launchings of powerful rockets, among them launch vehicles (LV). Scientific interest in this problem is due to the fact that such launchings can be regarded as active experiments in the Earth's atmosphere, and they can be used in solving a wide variety of problems in the physics of the ionosphere and radio wave propagation.

These investigations have also important practical implications since they furnish a means of substantiating reliable signal indications of technogenic effects (among them, unauthorized), which is necessary for the construction of an effective global radiophysical subsystem for detection and localization of these effects. Essentially, existing global systems of such a purpose use different processing techniques for infrasound and seismic signals. However, in connection with the expansion of the geography and of the types of technogenic impact on the environment, very challenging problems heretofore have been those of improve the sensitivity of detection and the reliability of measured parameters of the sources of impacts, based also on using independent measurements of the entire spectrum of signals generated during such effects.

To solve the above problems requires reliable information about fundamental parameters of the ionospheric response of the shock wave, such as the amplitude and the form, the period, the phase and group velocity of the wavetrain, as well as angular characteristics of the wave vector. Note that for the designating the ionospheric response of the shock wave, the literature uses terminology incorporating a different physical interpretation, among them the term 'shock-acoustic wave' (SAW) — Nagorsky (1998). For convenience, in this paper we shall use this term despite the fact that it does not reflect essentially the physical nature of the phenomenon.

Published data on fundamental parameters of the SAW differ greatly. According to a review by Karlov et al. (1980), the oscillation period of the ionospheric response of the SAW, recorded during launchings of the Apollo mission rockets, varied from 6 to 90 min, and the propagation velocity was in the range from 600 to 1670 m/s. The added complication is also that following the first SAW response arriving at the detection point, a 'second' wave propagating with the sound velocity at the ground level is often recorded (Karlov et al., 1980; Calais and Minster,

1996). A 'third' wave with large periods and subsonic propagation velocities is occasionally also detected (Nagorsky, 1998; 1999). This wave is identified as an exciting Acoustic-Gravity Wave (AGW) during a rocket launching.

There is an even greater uncertainty in the localization of the region of SAW generation, which is necessary both for an understanding of the physical mechanisms of the phenomenon, and for a scientific justification of the solution of applied problems. Published data are discussed in more detail in Section 5, by comparison with our obtained results.

The lack of comprehensive, reliable data on SAW parameters is due primarily to the limitations of existing experimental methods and detection facilities. The main body of data was obtained by measuring the frequency Doppler shift at vertical and oblique-incidence ionospheric soundings in the HF range (Jacobson and Carlos, 1994; Nagorsky, 1998). In some instances the sensitivity of this method is sufficient to detect the SAW reliably; however, difficulties emerge when localizing the region where the detected signal is generated. These problems are caused by the multiple-hop character of HF signal propagation. This gives no way of deriving reliable information about the phase and group velocities of SAW propagation, estimating angular characteristics of the wave vector, and, further still, of localizing the SAW source.

Using the method of transionospheric sounding with VHF radio signals from geostationary satellites, a number of experimental data on SAW parameters were obtained in measurements of the Faraday rotation of the plane of signal polarization which is proportional to a total electron content (TEC) along the line connecting the satellite-borne transmitter with the receiver (Mendillo, 1981; 1982; Li et al., 1994). A serious limitation of methods based on analyzing signals from geostationary satellites is that their number is too small and ever decreasing with time, and the distribution in longitude is non-uniform; this is especially true in regard to the eastern hemisphere. Published data from incoherent scatter (IS) radars are also scarce; as far as our knowledge goes, there is only one publication (Noble, 1990) reporting the detection of long-period (gravity) waves over the Arecibo IS station, following the launching of the Space Shuttle LV on October 18, 1993.

A common limitation of the above-mentioned methods when determining the SAW phase velocity is the necessity of knowing the time of a rocket launching since this velocity is inferred from the SAW delay with respect to the launch time assuming that the velocity is constant along the propagation path, which is quite contrary to fact.

For determining the above-mentioned reasonably complete set of SAW parameters, it is necessary to have appropriate spatial and temporal resolution which cannot be ensured by existing, very sparse, networks of ionozondes, oblique-incidence radio sounding paths, and IS radars. Furthermore, the creation of these facilities involves developing dedicated equipment, including powerful radio transmitters which contaminate the radio medium. As a result, the above sys-

tems cannot serve as an efficient basis for a global radiophysical subsystem for detection and localization of technogenic effects which must provide a continuous, global monitoring.

The advent and evolution of a Global Positioning System, GPS, and also the creation on its basis of widely branched networks of GPS stations (at least 600 sites at the end of 1999, the data from which are placed on the INTERNET) opened up a new era in remote ionospheric sensing. In the immediate future this network will undergo a substantial expansion by integration with the GLONASS positioning system (Klobuchar, 1997). In addition, researchers have also access to a standard software which permits them to unify a preprocessing of the data from multichannel two-frequency GPS receivers. In this context, a major effort must go into experimental and theoretical explorations of the possibilities of detecting technogenic perturbations of the ionosphere, as well as into the development of appropriate algorithms and software for a reprocessing of the data from GPS networks.

Currently some authors have embarked on an intense development of methods for detecting the ionospheric response of strong earthquakes (Calais and Minster, 1995), rocket launchings (Calais and Minster, 1996), and industrial surface explosions (Fitzgerald, 1997; Calais et al., 1998a; Calais et al., 1998b). In the cited references the SAW phase velocity was determined by the 'crossing' method by estimating the time delay of SAW arrival at subionospheric points corresponding to different GPS satellites observed at a given time. However, the accuracy of such a method is rather low because the altitude at which the subionospheric points are specified, is determined in a crude way.

The goal of this paper is to develop a method for determining SAW parameters (including the phase velocity, angular characteristics of the SAW wave vector, the direction towards the source, and the source location) using GPS-arrays whose elements can be chosen out of a large set of GPS stations of a global IGS network. Contrary to existing radio techniques, this method estimates SAW parameters without a priori information about the location and time of a rocket launching.

The emphasis in this paper is on the ionospheric response of the SAW which is recorded as a 'first' wave, although our developed methods make it also possible to analyze other wave manifestations of rocket launchings. This will be the subject of future work.

Section 2 presents a description of the geometry of experiments and general information about the LV launchings from the Baikonur and Kennedy Space Center (KSC) cosmodromes which are analyzed in this study. A brief account of the proposed method is presented in Section 3. Measurements of SAW parameters at different GPS-arrays during rocket launchings are discussed in Section 4. Section 5 discusses experimental results and compares them with the data reported by other authors. It is beyond the scope of this paper to consider the physical mechanisms of SAW generation and propagation.

2 The geometry and general characterization of experiments

This paper presents the results derived from determining the key SAW parameters during ascents of the Proton and Space Shuttle launch vehicles (LV) from cosmodromes Baikonur ($45.6°N$, $63.3°E$) and KSC ($28.5°N$, $279.3°E$) in 1998 and 1999 (a total of five launchings).

In spite of the large number of GPS stations, the selection of GPS-arrays for detecting SAW generated during rocket launchings is made difficult by the fact that the LV flight paths for both cosmodromes pass either over the Atlantic ocean (Space Shuttle LV) or over sparsely populated regions of Kazakhstan (Proton LV). Nevertheless, it was possible to utilize a sufficient number of GPS stations in order for this method to be implemented. Table 1 presents the geographic coordinates of the GPS stations used as GPS-array elements.

Fig. 1 portrays the geometry of experiments during Proton LV launchings from the Baikonur cosmodrome. The dash line roughly corresponds to the horizontal projection of the rocket flight trajectory with orbital inclination $\psi = 51.6°$ (Nagorsky, 1999). The symbol $\diamond$ marks the pad site. Bold dots mark the position of GPS stations, and upper-case lettering corresponds to their names. The scaling of the coordinate axes is selected from considerations of an approximate equality of the linear dimensions along the latitude and longitude.

Below is a summary of results derived from detecting one standard launching (on November 20, 1998) and two abortive launchings (July 5 and October 27, 1999) of the Proton LV. The following information about rocket launchings from the Baikonur Cosmodrome as extracted from the INTERNET sites: http//www.flatoday.com; http://www.spacelaunchnews.com; and http://www.ksc.nasa.gov. Official data on abortive Proton LV launches on July 5 and October 27, 1999 were taken from the English version of the press release issued by the Khrunichev Center which is available on: http://www.isllaunch.com.

A Proton launch vehicle failed during launch on July 5, 1999 (Day 186). Initial analyses indicated a malfunction of the Proton's second stage. Liftoff took place at 13:32 UT from a launch pad of the Baikonur Cosmodrome. First stage flight was normal, with second stage separation and ignition on time. Telemetry first reported anomalous data at approximately 280 seconds into the flight, with deviations from the planned trajectory appearing on ground tracking systems by 330 seconds. By 390 seconds the LV was 14 km below its planned trajectory. Ground systems tracked the upper stages and payload to impact. The Proton's third stage, with the upper stage and its Raduga spacecraft payload, fell in the Karaganda region of Kazakhstan.

The Proton LV was launched from a launch pad at Baikonur Cosmodrome on October 27 (Day 300), 1999 at 16:16 UT. Based on preliminary data, failure of one of the main second stage engines occurred 222 seconds after liftoff, followed

by failure of all engines of the stage. The second stage together with the upper stage and satellite fell back to earth in the Karaganda region of Kazakhstan.

In a typical Proton launch, the vehicle's six first-stage engines ignite 1.6 s before liftoff. Stage two ignition occurs approximately two minutes into flight, four seconds prior to jettison of the first stage. Stage three vernier engine ignition occurs at 330 seconds, with separation of the second and third stages taking place 3.5 s later. The stage three main engine ignition occurs 2.5 s after separation.

Unfortunately, we were unable to obtain more detailed information about the LV launch schedule on the above days. However, for a further analysis we need only know that these failures occurred after the second stage was in operation longer than 200 s and 100 s for the July 5 and October 27, 1999 launches, respectively.

General information regarding these launches, as well as the scheduled launch of November 20, 1998 (Day 324) is summarized in Table 2 (including the start time t_0 of UT, the start time of LT for one of the GPS-array sites, the orbital inclination ψ to the equatorial plane, and the level of geomagnetic disturbance according to Dst-variation data). It was found that the deviation of Dst for the selected days was quite moderate thus enabling the SAW to be identified.

Fig. 2 presents the experimental geometry during Space Shuttle LV launchings from the KSC Cosmodrome (the designations are the same as in Fig. 1). The Space Shuttle Discovery spacecraft (STS-90) and Space Shuttle Columbia (STS-95) were launched on April 17 (Day 107) and on October 29 (Day 302), respectively. General information about these launches is also summarized in Table 2. The horizontal projection of the rocket trajectory for the October 29 launching is constructed using the INTERNET data. The level of geomagnetic disturbance as deduced from the Dst-variation data was also found to be quite moderate for these launches, which made it possible to reliably identify the SAW.

3 Methods of determining shock-acoustic wave characteristics using GPS-arrays

The standard GPS technology provides a means for wave disturbances detecion based on phase measurements of TEC at each of spaced two-frequency GPS receivers. A method of reconstructing TEC variations from measurements of the ionosphere-induced additional increment of the group and phase delay of the satellite radio signal was detailed and validated in a series of publications (Calais and Minster, 1995, 1996; Fitzgerald, 1997). We reproduce here only the final formula for phase measurements

$$I = \frac{1}{40.308} \frac{f_1^2 f_2^2}{f_1^2 - f_2^2} [(L_1\lambda_1 - L_2\lambda_2) + const + nL] \qquad (1)$$

where $L_1\lambda_1$ and $L_2\lambda_2$ are additional paths of the radio signal caused by the phase delay in the ionosphere, (m); L_1 and L_2 represent the number of phase rotations at the frequencies f_1 and f_2; λ_1 and λ_2 stand for the corresponding wavelengths, (m); *const* is the unknown initial phase ambiguity, (m); and nL are errors in determining the phase path, (m).

Phase measurements in the GPS can be made with a high degree of accuracy corresponding to the error of TEC determination of at least 10^{14} $^{-2}$ when averaged on a 30-second time interval, with some uncertainty of the initial value of TEC, however (Hofmann-Wellenhof et al., 1992). This makes possible detecting ionization irregularities and wave processes in the ionosphere over a wide range of amplitudes (up to 10^{-4} of the diurnal TEC variation) and periods (from 24 hours to 5 min). The unit of TEC, which is equal to 10^{16} $^{-2}$ ($TECU$) and is commonly accepted in the literature, will be used in the following.

Fig. 3a gives a schematic representation of the transionospheric sounding geometry. The axes z, y, and x are directed, respectively, zenithward, northward (N) and eastward (E). P — point of intersection of Line-of-Sight (LOS) to the satellite with the maximum of the ionospheric $F2$-region; S — subionospheric point; α_s —the azimuthal angle, counted off from the northward in a clockwise direction; and θ_s —the angle of elevation between the direction r along LOS and the terrestrial surface at the reception site.

In some instances a convenient way of detecting and determining the ionospheric response delay of the shock wave involves inferring the frequency Doppler shift F from TEC series obtained by formula (1). Such an approach is also useful in comparing TEC response characteristics from the GPS data with those obtained by analyzing VHF signals from geostationary satellites, as well as in detecting the shock wave in the HF range. To an approximation sufficient for the purpose of our investigation, a corresponding relationship was obtained by K. Davies (1969)

$$F = 13.5 \times 10^{-8} I'_t / f \tag{2}$$

where I'_t stands for the time derivative of TEC. Relevant results derived from analyzing the $F(t)$-variations calculated for the 'reduced' frequency of 136 MHz are discussed in Section 4.

The correspondence of space-time phase characteristics, obtained through transionospheric soundings, with local characteristics of disturbances in the ionosphere was considered in detail in a wide variety of publications (Bertel et al., 1976; Afraimovich et al., 1992; Mercier and Jacobson, 1997) and is not analyzed at length in this study. The most important conclusion of the cited references is the fact that, as for the extensively exploited model of a 'plane phase screen' disturbances $\Delta I(x, y, t)$ of TEC faithfully copy the horizontal part of the corresponding disturbance $\Delta N(x, y, z, t)$ of local concentration, independently of the

angular position of the source, and can be used in experiments on measuring the wave disturbances of TEC.

However, the TEC response amplitude experiences a strong azimuthal dependence caused by the integral character of a transionospheric sounding. As a first approximation, the transionospheric sounding method is responsive only to TIDs with the wave vector K_t perpendicular to the direction r. A corresponding condition for elevation θ and azimuth α of an arbitrary wave vector K_t normal to the direction r, has the form

$$\theta = \arctan(-\cos(\alpha_s - \alpha)/\tan\theta_s) \tag{3}$$

We used formula (3) in determining the elevation θ of K_t from the known mean value of azimuth α by Afraimovich et al. (1998) – see Sections 3.2 and 4.

3.1 Detection and determination of the horizontal phase velocity V_h and the direction α of the SAW phase front along the ground by GPS-arrays

In the simplest form, space-time variations of the TEC $\Delta I(t, x, y)$ in the ionosphere, at each given time t can be represented in terms of the phase interference pattern that moves without a change in its shape (the solitary, plane travelling wave)

$$\Delta I(t, x, y) = \delta \sin(\Omega t - K_x x - K_y y + \varphi_0) \tag{4}$$

where δ, K_x, K_y, Ω — are the amplitude, the x- and y-projections of the wave vector $\boldsymbol{K}$, and the angular frequency of the disturbance, respectively; $T = 2\pi/\Omega$, $\Lambda = 2\pi/|K|$ is its period and wavelength; and φ_0 is the initial phase of the disturbance. The vector K is a horizontal projection of the full vector K_t (Fig. 3a).

At this point, it is assumed that in the case of small spatial and temporal increments (the distances between GPS-array sites are less than the typical spatial scale of TEC variation, and the time interval between counts is less than the corresponding time scale), the influence of second derivatives can be neglected. The following choices of GPS-arrays all meet these requirements.

For the SAW which have mostly the character of an N-wave (Li et al., 1994; Calais and Minster, 1995, 1996; Fitzgerald, 1997; Calais et al., 1998), the amplitude δ in (4) can be specified as (with an appropriate choice of the model parameters)

$$\delta(t) = \exp[-(\frac{t - t_{max}}{t_d})^2] \tag{5}$$

where t_{max} is the time when the disturbance has a maximum amplitude, and t_d is the half-thickness of the 'wave packet'. We employed this model in simulating

the SAW detected during Proton LV launch on July 5, 1999 (at the left of Fig. 4, and at the right of Fig. 5).

We now summarize briefly the sequence of data processing procedures. Out of a large number of GPS stations, three sites (A,B,C) are selected, the distances between which do not exceed about one-half the expected wavelength Λ of the perturbation. Site B is taken to be the center of a topocentric reference frame whose axis x is directed eastward, and the axis y is directed northward. The receivers in this frame of reference have the coordinates (x_A, y_A), (0,0), (x_C, y_C). Parallel lines in Fig. 3b are lines of equal TEC; the arrow indicates the direction α of a normal to these lines, that is, the direction of the wave vector K. Such a configuration of the GPS receivers represents the GPS-array with a minimum number of the required elements. In regions with a dense network of GPS sites, we can obtain a large variety of GPS-arrays of a different configuration enabling the acquired data to be checked for reliability; in this paper we have exploited such a possibility.

The input data include series of the 'oblique' value of TEC $I_A(t)$, $I_B(t)$, $I(t)$, as well as corresponding series of values of the elevation $\theta_s(t)$ and the azimuth $\alpha_s(t)$ of the beam to the satellite calculated using our developed CONVTEC software program which converts the RINEX-files, standard for the GPS system, from the INTERNET (Gurtner, 1993). For determining SAW characteristics, continuous series of measurements of $I_A(t)$, $I_B(t)$, $I_C(t)$ are selected with a length of at least a one-hour interval which includes the start time.

To eliminate variations of the regular ionosphere, as well as trends introduced by orbital motion of the satellite, a procedure is used to remove the linear trend involving a preliminary smoothing of the initial series with the selected time window. This procedure is best suited to the detection of the signal such as a single pulse (N-wave) when compared to the frequently used band-pass filter (Li et al., 1994; Calais and Minster, 1995, 1996; Fitzgerald, 1997; Calais et al., 1998). A limitation of the band-pass filter is the delay and the oscillatory character of the response which gives no way of reconstructing the form of the N-wave.

Series of the values of the elevation $\theta_s(t)$ and azimuth $\alpha_s(t)$ of the beam to the satellite are used to determine the location of the subionospheric point S (see Fig. 3a), as well as to calculate the elevation θ of the wave vector K_t of the disturbance from the known azimuth α (see formula (3) and Section 4.2).

The most reliable results from the determination of SAW parameters correspond to high values of elevations $\theta_s(t)$ of the beam to the satellite because sphericity effects become reasonably small. In addition, there is no need to recalculate the 'oblique' value of TEC $\Delta I(t)$ to the 'vertical' value. In this paper, all results were obtained for elevations $\theta_s(t)$ larger than 30°.

Since the distance between GPS-array elements (from several tens of kilometers to a few thousand kilometers) is much smaller than that to the GPS satellite (over 20000 km), the array geometry at the height h_{max} is identical to that on the ground.

Fig. 4a shows typical time dependencies of an 'oblique' TEC $\Delta I(t)$ at the GPS-array CHUM station near the Baikonur Cosmodrome for the start day, July 5, 1999 (heavy curve), one day before and after the start (thin lines). For the same days; panel b shows TEC variations $\Delta I(t)$ with the removed linear trend and a smoothing with the 5-min time window. Variations in frequency Doppler shift $F(t)$; 'reduced' to the sounding signal frequency of 136 MHz, for three sites of the array (SELE, CHUM, SHAS) for the launch day, July 5, 1999, are presented in panel c. Day numbers, GPS station names and GPS PRN satellite numbers are indicated in all panels. The arrows at the abscissa axis indicate the start time t_0.

It is evident from Fig. 4 that fast N-shaped oscillations with a typical period T of about 300 s are clearly distinguished among slow TEC variations. The oscillation amplitude (up to 0.5 $TECU$) is far in excess of the TEC fluctuation intensity during 'background' days. Variations in frequency Doppler shift $F(t)$ for spatially separated sites (SELE, CHUM, SHAS) are well correlated but are shifted relative to each other by an amount well below the period, which permits the SAW propagation velocity to be unambiguously determined. A time resolution of 30 s used in our study, which is standard for the GPS data, is not quite sufficient for determining small shifts of such signals with an adequate accuracy for different sites of the array (Fig. 4c). Therefore, we used a parabolic approximation of the $F(t)$-oscillations in the neighborhood of minimum $F(t)$, which is quite acceptable when the signal/noise ratio is high. In addition, we used different combinations for three sites of the possible number of GPS-array sites in the area of Baikonur and KSC Cosmodromes. Relevant results for all combinations are presented in Table 3.

With proper account of a good signal/noise ratio (larger than 1), we determine the horizontal projection of the phase velocity V_h with the known coordinates of array sites A, B, C from time t_p shifts of a maximum deviation of the frequency Doppler shift $F(t)$. Preliminarily measured shifts are subjected to a linear transformation with the purpose of calculating shifts for sites spaced relative to the central site northward N and eastward E. This is followed by a calculation of the E- and N-components of V_x and V_y, as well as the direction α in the range of angles 0°–360° and the modulus V_h of the horizontal component of the SAW phase velocity

$$\begin{aligned} \alpha &= \arctan(V_y/V_x) \\ V_h &= |V_x V_y|(V_x^2 + V_y^2)^{-1/2} \end{aligned} \tag{6}$$

where V_y, V_x are the velocities with which the phase front crosses the axes x and y. The orientation α of the wave vector K, which is coincident with the propagation azimuth of the SAW phase front, is calculated unambiguously in the range 0°–360° subject to the condition that $\arctan(V_y/V_x)$ is calculated having regard to the sign of the numerator and denominator.

The above method for determining the SAW phase velocity neglects the correction for orbital motion of the satellite because the estimates of V_h obtained

below exceed an order of magnitude as a minimum the velocity of the subionospheric point at the height h_{max} for elevations $\theta_s > 30^\circ$ (Afraimovich et al., 1998).

From the delay $\Delta t = t_p - t_0$ and the known path length between the launch pad and the subionospheric point we calculated also the SAW mean velocity V_a in order to compare our obtained estimates of the SAW phase velocity with the usually used method of measuring this quantity.

3.2 Determination of the elevation of the wave vector θ and the velocity modulus V_t of the shock wave

Afraimovich et al. (1992) showed that for an exponential ionization distribution the TEC disturbance amplitude (M) is determined by the aspect angle γ between the vectors K_t and r (see Fig. 3a), as well as by the ratio of the wavelength of the disturbance Λ to the half-thickness of the ionization maximum h_d

$$M \propto \exp\left(-\frac{\pi^2 h_d^2 \cos^2\gamma}{\Lambda^2 \cos^2\theta_s}\right) \tag{7}$$

where θ_s is the elevation of the wave vector r.

In the case under consideration (see below), for the phase velocity of order 1 km/s and for the period of about 200 s, the wavelength Λ is comparable with the half-thickness of the ionization maximum h_d. When the elevations θ_s are 30°, 45°, 60° , the 'beam-width' $M(\gamma)$ at 0.5 level is, respectively, 25°, 22° and 15°. If h_d is twice as large as the wavelength, then the beam tapers to 14°, 10° and 8°, respectively.

The beam-width is sufficiently small that the aspect condition (3) restricts the number of beam trajectories to the satellite, for which it is possible to detect reliably the SAW response in the presence of noise (near the angles $\gamma = 90^\circ$). On the other hand, formula (**??**) can be used to determine the elevation θ of the wave vector K_t of the shock wave at the known value of the azimuth α (Afraimovich et al., 1998). Hence the phase velocity modulus V_t can be defined as

$$V_t = V_h \times sec(\theta) \tag{8}$$

The above values of the width $M(\gamma)$ determine the error of calculation of the elevations θ (of order 20° to the above conditions (Section 3.3).

3.3 Determining the position and 'switch-on' time of the SAW source without regard for refraction corrections

The ionospheric region that is responsible for the main contribution to TEC variations lies in the neighborhood of the maximum of the ionospheric F-region, which does determine the height h_{max} of the subionospheric point. When selecting

h_{max}, it should be taken into consideration that the decrease in electron density with height above the main maximum of the F_2-layer proceeds much more slowly than is the case below the maximum. Since the density distribution with height is essentially a 'weight function' of the TEC response to a wave disturbance (Afraimovich et al., 1992), it is appropriate to use, as h_{max}, the value exceeding the true height of the layer h_{F2} maximum by about 100 km. h_{F2} varies over a reasonably wide range (250–350 km) depending on the time of day and on some geophysical factors which, when necessary, can be taken into account if corresponding additional experimental data and current ionospheric models are used. In all calculations that follow, $h_{max} = 400$ km is used.

To a first approximation, it can be assumed that it is at this altitude where the imaginary detector is located, which records the ionospheric SAW response in TEC variations. The 'horizontal size' of the detection region, which can be inferred from the propagation velocity of the subionospheric point as a consequence of the orbital motion of the GPS satellite (of order 50 m/s), and from the SAW period (of order 300 s — see Section 4), does not exceed 15–20 km, which is far smaller than the 'vertical size'.

From the GPS data we can determine the coordinates X_s and Y_s of the subionospheric point in the horizontal plane $X0Y$ of a topocentric frame of reference centered on the point B(0,0) at the time of a maximum TEC deviation caused by the arrival of the SAW at this point (see Fig. 3a). Since we know the angular coordinates θ and α of the wave vector K_t, it is possible to determine the location of the point at which this vector intersects the horizontal plane $X'0Y'$ at the height h_w of the assumed source. Assuming a rectilinear propagation of the SAW from the source to the subionospheric point and neglecting the sphericity the coordinate X_w and Y_w of the source in a topocentric frame of reference can be defined as

$$X_w = X_p - (h_{max} - h_w)\,\frac{\cos\theta\sin\alpha}{\sin\theta} \tag{9}$$

$$Y_w = Y_p - (h_{max} - h_w)\,\frac{\cos\theta\cos\alpha}{\sin\theta} \tag{10}$$

The coordinates X_w and Y_w, thus obtained, can readily be recalculated to the values of the latitude and longitude (ϕ_w and λ_w) of the source.

For SAW generated during earthquakes, industrial explosions and underground tests of nuclear devices, h_w is taken to be equal to 0 (the source lying at the ground level). When recording SAW produced by launchings of powerful rockets, the region of SAW generation can lie at heights h_w of order 100 km or higher (Li et al., 1994; Nagorsky, 1998).

Using this approximation we neglect the possible refraction at the SAW propagation from the source to the height h_{max}. In some publications (Calais et al., 1998) this problem is solved by performing trajectory calculations using standard '*ray tracing*' procedures and neutral atmosphere models. In doing so,

'*ray tracing*' calculations were carried out from the source. In this study it is also possible to perform such calculations, not from the source but from the subionospheric point (return trajectory).

It should be noted, however, that according to our data (Section 4) and to the conclusions of some authors (Li et al., 1994; Nagorsky, 1998), the source lies at 100 km altitude at least. Thus the region of SAW generation is within the narrow height range (90–150 km) where the sound velocity gradient is maximal (Li et al., 1994). Within the approximation of 'short' waves (geometrical optics), this condition would mean the significance of refraction effects. However, the radial size of the region of SAW formation, like the extent of the disturbance itself which it generated by the rocket jet, is about 30–50 km at the above-mentioned heights. This value is comparable with the typical scale of variation of the sound velocity with height, hence the wave is no longer a 'short' one, and the geometrical optics approximation is inapplicable. One would therefore expect that the refraction effect in the neighborhood of the SAW source will be smaller than anticipated in terms of geometrical optics.

Given the coordinates of the subionospheric point and of the disturbance source, the mean value of the SAW propagation velocity between the source and the subionospheric point, and the arrival time of the SAW at this point, then within the approximation of a rectilinear propagation it is easy to determine the 'switch-on' delay Δt_w of the anticipated SAW source with respect to the start. This would make it possible to obtain additional information about the SAW source which is needed to understand the mechanism of SAW generation. The estimates of Δt_w made below assume that the propagation velocity is taken equal to 700 m/s (see Li et al., 1994). Note that by the 'switch-on' time of the source is meant here the time of a maximum disturbance of the background state of the medium when the SAW is generated.

4 Results of measurements

Hence, using the transformations described in Section 3, we obtain the following parameters determined from TEC variations and characterizing the SAW: t_0 — start time; t_p — time of a maximum deviation of the frequency Doppler shift $F(t)$; Δt — delay of t_p with respect to t_0; T — SAW period; A_I — TEC disturbance amplitude; A_F — amplitude of a maximum frequency Doppler shift at the 'reduced' frequency of 136 MHz; α and θ — azimuth and elevation of the wave vector K_t; V_h and V_t — horizontal component and modulus of the phase velocity; V_a — mean wave velocity calculated from the delay Δt and from the known path-length between the launch pad and the subionospheric point; ϕ_w and λ_w — latitude and longitude of the source at 100km altitude; and Δt_w — 'switch-on' delay of the assumed SAW source with respect to the start.

Corresponding values of the SAW parameters, and also site names of the GPS-array and GPS satellite PRN numbers are presented in Table 3 for Baikonur Cosmodrome and Table 4 for the KSC Cosmodrome.

It should be noted that the estimates of A_I and A_F are obtained by filtering 'oblique' TEC series; therefore, equivalent estimates for 'vertical' TEC are smaller by a factor varying from 1 to 2 depending on the elevation θ_s of the beam to the satellite.

Solid curves in Figs. 1 and 2 show trajectories of subionospheric points for each of the GPS satellites at the height $h_{max} = 400$ km. Dark diamonds along the trajectories correspond to the coordinates of subionospheric points at the time t_p of a maximum deviation of the frequency Doppler shift F (Fig. 4c). Asterisks designate the source location at 100 km altitude inferred from the GPS-array data. Numbers at the asterisks refer to the corresponding day numbers and to the 'switch-on' delay of the source with respect to the start time. Dashed straight lines connecting the anticipated source with the subionospheric point show the horizontal projection of the wave vector K_t (see Fig. 3a).

4.1 SAW parameters during Proton LV launches from Baikonur Cosmodrome

Let us consider the results derived from analyzing the ionospheric effect of SAW during failed Proton LV launch on July 5, 1999 (line 2 in Table 2) obtained at the array (SELE, CHUM,SHAS) for PRN14 (at the left of Fig. 4, and line 1 in Table 3).

In this case the delay of the SAW response with respect to the start time is 12 min. The SAW has the form of an N-wave with a period T of about 300 s and an amplitude $A_I = 0.5\ TECU$, which is an order of magnitude larger than TEC fluctuations for background days. It should be noted, however, that this time interval was characterized by a very low level of geomagnetic activity (11 nT).

The amplitude of a maximum frequency Doppler shift A_F at the 'reduced' frequency of 136 MHz was found to be 0.12 Hz. In view of the fact that the shift F is inversely proportional to the sounding frequency squared (Davies, 1969), this corresponds to a Doppler shift at the working frequency of 13.6 MHz and the equivalent oblique-incidence sounding path of about $A_F = 12$ Hz.

The azimuth and elevation α and θ of the wave vector K_t whose horizontal projection is shown in Fig. 1 by a dashed line and is marked by K_1, are 153° and 59°, respectively. The horizontal component and the modulus of the phase velocity were found to be $V_h = 1808$ m/s and $V_t = 931$ m/s. The source coordinates at 100 km altitude were determined as $\phi_w = 48°$ and $\lambda_w = 66°$.

The 'switch-on' delay of the SAW source Δt_w with respect to the start time was 264 s. The 'mean' velocity of about $V_a = 1000$ m/s, determined in a usual

manner from the response delay with respect to the start, was close the phase velocity V_t.

Similar results for the array (POL2, CHUM, SHAS) and PRN09 were also obtained for failed launch of October 27, 1999. They correspond to the projection of the vector K_2 in Fig. 1, to the time dependencies in Fig. 4 (at the right), and to line 7 in Table 3. One can only note that the SAW amplitude was by a factor of 4–5 smaller than that for launch of July 5, 1999. At an increased level of magnetic activity (–80 nT) this led to a smaller (compared to July 5, 1999) signal/noise ratio, which, however, did not interfere with obtaining reliable estimates of SAW parameters.

Fig. 5 (at the right) and line 12 of Table 3 present data for standard launch of the Proton LV on November 20, 1998. A corresponding projection of the vector K_3 is shown in Fig. 1. A comparison of the data for standard launch November 20, 1998 and failed launches showed that SAW parameters were reasonably similar, irrespective of the level of geomagnetic disturbance, the season, and the local time.

4.2 SAW parameters during Space Shuttle launches from the KSC Cosmodrome

Let us consider the results derived from analyzing the ionospheric effect of the SAW during Space Shuttle LV launch on October 29, 1998 (line 3 of Table 2) obtained at the array (AOML, KYW1, EKY1) for PRN01 (at the left of Fig. 5, and line 1 in Table 4).

As in the case of Proton LV launches, the delay of the SAW response with respect to the start time is 12 min. The SAW has the form of an N-wave with a period T of about 210 s and an amplitude $A_I = 0.3\ TECU$ (for AOML), which is an order of magnitude larger than TEC fluctuations for background fields. The amplitude of a maximum frequency Doppler shift A_F at the 'reduced' frequency of 136 MHz was found to be 0.07 Hz (for AOML). It should be noted, however, that this time interval was characterized by a very low level of geomagnetic activity (–15 nT).

The azimuth and elevation α and θ of the wave vector K_t whose horizontal projection is shown in Fig. 2 by a dashed line and is marked by K_1 are 214° and 34.7°, respectively. The horizontal component and the modulus of the phase velocity, and the mean velocity V_a are similar for those of the Proton LV (see Table 4). The source coordinates at 100 km altitude are determined as $\phi_w = 28.5°$ and $\lambda_w = 284°$. The 'switch-on' delay of the SAW source Δt_w with respect to the start time is 204 s.

4.3 Verifying the reliability of measurements of SAW parameters

To convince ourselves that the determination of the main parameters of the SAW form and dynamics is reliable for the launches analyzed here, in the area of the Baikonur and KSC Cosmodromes we selected different combinations of three sites out of the sets of GPS stations available to us, and these data were processed with the same processing parameters. Relevant results for Baikonur (including the average results for the sets Σ), presented in Table 3 and in Fig. 1 (SAW source position), show that the values of SAW parameters are similar, which indicates a good stability of the data obtained, irrespective of the GPS-array configuration.

The relative position of the Proton LV flight path and of the GPS-array stations suitable for SAW detection was very convenient for our experiment because the subionospheric points of the GPS satellites were close to the portion of the trajectory where the anticipated SAW source was located (Li et al., 1994; Nagorsky, 1998), and away from the launch pad. In addition, the aspect condition (3) corresponding to a maximum amplitude of the SAW response to the SAW passage was satisfied quite well for this geometry for all array stations simultaneously. This is confirmed by a high degree of correlation of SAW responses at the array elements (Fig. 4c), which made it possible to obtain different sets of triangles from the six GPS stations available to us.

Unlike he Baikonur Cosmodrome, the relative position of the Space Shuttle LV flight path and of the GPS-array stations was inconvenient for SAW detection because the subionospheric points of the GPS satellites were near the launch pad. As a consequence the aspect condition (3) was not satisfied simultaneously for all GPS stations located near the Cosmodrome. This is especially true for stations CCV1, CCV3 and EKY1 located in the neighborhood of the launch pad along a direction similar to that of the LV flight path. This resulted in a low degree of correlation and a very different amplitude of SAW responses at the array elements (Fig. 5f). Some of the stations listed in Table 1 are too close to each other (CCV1, CCV3; MIA1, MIA3; KYW1, KYW2) and cannot be used in mutual verification of the reliability of measurements. As a result, we were able to obtain, for the October 29, 1998 launch, only two sets of triangles out of the nine GPS stations available to us (see Table 4).

Because of the low correlation of the responses and the inconvenient GPS-array geometry for the April 17, 1998 launch, we were also unable to obtain reliable estimates of the SAW wave vector parameters. Therefore, we did not plot the relevant data in Fig. 2 and limited ourselves to mentioning them in Table 4 (lines 4 and 5).

We availed ourselves also of another method to check the data from the GPS-array for reliability, namely, a modeling using the algorithm for calculating TEC along the 'receiver-satellite' beam for a typical model of the regular ionosphere, a disturbed SAW with specified properties described by Afraimovich et al. (1998).

A peculiarity of this algorithm is that it is possible to calculate TEC for a particular selected array and for a real trajectory of the satellite determined by the initial navigational RINEX-file.

As an example, Fig. 5 (left) shows the computed data for the array (SELE, CHUM, SHAS) and for the SAW model in the form of wave packet (5) with a period of 240 s, the packet's duration of 240 s, a maximum amplitude of 0.5 $TECU$, the horizontal phase velocity $V_h = 1200$ m/s, and the azimuth α and the elevation θ of the wave vector K_t equal to 153° and 60°, respectively. A comparison of the parameters specified in the modeling procedure with those obtained by processing the data of TEC $I(t)$ model series shows that these values agree with an accuracy no worse than 10%. Noteworthy also is a good agreement of experimental (at the left of Fig. 4) and model (at the left of Fig. 5) TEC variations $\Delta I(t)$ and $F(t)$ for the array (SELE, CHUM, SHAS).

5 Discussion

Here we discuss the main results and compare them with findings reported by other authors. Within the context of this study we deliberately pass over a physical interpretation of our obtained results because of no information available about the dynamics and energetics of Proton and Space Shuttle LV launches. Our intention is to obtain more trustworthy and reliable data ensuring the new possibilities of a global GPS monitoring.

5.1 The form of response

It was found that in spite of the difference of LV characteristics, the local time, the season, and the level of geomagnetic disturbance, the ionospheric response for all launches has the character of an N-wave. The SAW period T is 270–360 s, and the amplitude exceeds the standard deviation of background TEC fluctuations in this range of periods under quiet and moderate geomagnetic conditions, by a factor of 2–5 as a minimum.

Our measurements of the period and amplitude of the SAW response are in good agreement with frequency Doppler shifts measured in the HF range during Space Shuttle LV launches on February 28, 1990 and April 28, 1991 (Jacobson and Carlos, 1994), as well as wit corresponding estimates of a maximum shift F reported by Nagorsky (1998, 1999) for oblique HF radio path during LV launches from Baikonur Cosmodrome. They are also similar to the estimates obtained by Li et al. (1994) using the transionospheric VHF radio signal from geostationary satellite MARECS-B2 during Space Shuttle LV launches on October 18, 1993 (STS-58) and February 3, 1994 (STS-60).

According to measurements reported by Calais and Minster (1996), during Space Shuttle (STS-58) launch on October 18, 1993 two series of TEC fluctuations

were recorded, one of which had also the form of an N-wave with a maximum amplitude of 0.25 TECU, which is also consistent with our data.

It was pointed out in the literature that SAW of a similar form and with a similar amplitude were detected during powerful industrial explosions (Afraimovich et al., 1984; Jacobson et al., 1988; Blanc and Jacobson, 1989; Fitzgerald, 1997; Calais et al., 1998a; 1998b; Nagorsky, 1998).

5.2 Angular characteristics of the wave vector, and the phase velocity of SAW

As pointed out in the Introduction, some researchers report markedly different values of the SAW propagation velocity — up to several thousand m/s, which exceeds the sound velocity at SAW propagation heights in the atmosphere. According to the data from a review by Karlov et al. (1980), the propagation velocity of the SAW ionospheric response recorded during launches of the Apollo mission rockets, varied from 600 to 1670 m/s.

Arendt (1971) suggested that the shock wave produced by rocket flight is divided in the ionosphere at about 160 km altitude into the ion-acoustic mode (with a velocity as high as 1.3 km/s) and a normal acoustic mode (with the velocity of up to 500 m/s). Arendt (1971) explains the difference in propagation velocities of the first and second disturbances observed during Apollo-14 and Apollo-15 launches at the same distance of 1440 km from the start site, by a difference in atmospheric conditions and propagation paths of the waves because of seasonal variations of the ionosphere.

Noble (1990) describes the observations of long-period waves over the Arecibo incoherent scatter station during Space Shuttle STS-4 launch on June 27, 1982. At a large distance from the path (up to 1000 km) the group velocity of wave propagation was found to be 600–700 m/s.

According to GPS measurements (Calais and Minster, 1996), the SAW phase velocity at ionospheric heights is about 1000–1300 m/s.

A common limitation of existing methods for determining the SAW phase velocity is the need to know the launch time of the rocket since this velocity is calculated from the SAW delay with respect to the start time assuming that the velocity along the propagation path is constant, which is by far contrary to fact. Furthermore, only the horizontal component of the phase velocity V_h was in essence determined in such studies. At different values of elevation of the wave vector K_t, the velocity V_h corresponds to markedly differing values of the modules of the phase velocity V_t.

The use of the method proposed in this paper makes possible determining angular characteristics of the wave vector K_t and, accordingly, estimating V_t. According to our data (Tables 3 and 4), the elevation of the SAW wave vector varied from 30–60°, and the SAW phase velocity was in the range of from 900

to 1200 m/s. We determine the phase velocity of the line of equal TEC at the height of the ionospheric F-region maximum which makes the main contribution to variations in TEC between the receiver and the GPS satellite and corresponds to the region of maximum sensitivity of the method. Since V_t approaches the sound velocity at these altitudes (Li et al., 1994), this makes it possible to identify the sound nature of a TEC perturbation.

5.3 The location and 'switch-on' delay of the SAW source

The position of the SAW source, calculated by neglecting refraction corrections, corresponds to the segment of the LV trajectory (Figs. 1 and 2) within distances of at least 700–900 km from the launch pad for the Proton LV and of at least 200–500 km for the Space Shuttle LV. This is consistent with the 'switch-on' delay Δt_w of the source which is 250–300 s for the Proton LV and 200 s for the Space Shuttle LV. As is evident from our data, the calculated position of the SAW source for rocket launches does not coincide with the position of the launch pad. At the same time the source location is in reasonably good agreement with that of horizontal projections of LV trajectories (Figs. 1 and 2).

Kaschak et al. (1970) analyzed the data from the infra sound measuring arrays located on the USA north-eastern coast which observed strong acoustic signals from launch and reentry areas of the Saturn-5 LV. The authors identified three types of signals: one includes early signals whose arrival time corresponded to supersonic values of their velocity equal to 500–1000 m/s; the other type represents normal signals with the group velocity approximately equal to the normal velocity of sound propagation in the air; and the last type involves late signals with subsonic velocities in the range of from 190 to 240 m/s. Kaschak et al. (1970) and Balachandran et al. (1971) suggested that the so-called 'early' signals during rocket launches are caused by SAW which are generated during the reentry of the first stage at distances from the launch pad exceeding 500 km.

However, our data are in better agreement with the mechanism substantiated by Li et al. (1994), Calais and Minster (1996), and Nagorsky (1998, 1999). They believe that the generation of SAW occurs during a nearly horizontal travel of the rocket with the operating engine along the acceleration segment of the trajectory, at the lower atmospheric heights of 100–130 km. The rocket travels this segment with supersonic velocity at 100–300 s of its flight at a distance of at least 500 km from the launch pad (see the data on the Proton LV flight schedule in Section 2). As soon as it ascends to an altitude of about 100 km, the SAW source is 'switched on'.

6 Conclusions

In this paper we have investigated the form and dynamics of shock-acoustic waves (SAW) generated during rocket launches. We have developed a method for determining SAW parameters (including angular characteristics of the wave vector and the SAW phase velocity, as well as the direction to the source) using the GPS-arrays whose elements can be chosen out of a large set of GPS stations forming part of a global IGS network. Unlike existing radio techniques, the proposed method estimates SAW parameters without a priory information about the site and time of rocket launch. The implementation of the method is illustrated by analyzing ionospheric effects from launches of the Proton and Space Shuttle LV from Baikonur and KSC Cosmodromes in 1998 and 1999 (totaling five launches).

The results reported in this study suggest the following conclusions:

1. In spite of the difference of LV characteristics, for all launches the ionospheric response has the character of an N-wave corresponding to the form of a shock wave, irrespective of the type of disturbance source (rocket launch, industrial explosion).

2. The SAW period T is 270–360 s, and its amplitude (from 0.1 to 0.5 $TECU$) exceeds the standard deviation of $TECU$ background fluctuations in this range of periods under quiet and moderate geomagnetic conditions by a factor of 2–5 as a minimum.

3. The elevation of the SAW wave vector varies within 35–60°, and the SAW phase velocity (900–1200 m/s) approaches the sound velocity at heights of the ionospheric F-region minimum. This makes it possible to identify the sound nature of a TEC perturbation.

4. The position of the SAW source, calculated by neglecting refraction corrections, corresponds to a segment of the Proton LV trajectory at a distance of at least 700–900 km from the launch pad and to the LV flight altitude of at least 100 km. For the Space Shuttle LV the position of the SAW source corresponds to the segment of the trajectory at a distance of at least 200–500 km from the launch pad and to the LV flight altitude of at least 100 km.

Hopefully, our investigation would provide additional useful insights into the physical processes occurring during flights of rockets in the Earth's atmosphere on the acceleration segment of the trajectory. In addition, this would make it possible to identify more reliable signal indications of technogenic effects which are necessary for constructing an effective global radio subsystem for detection and localization of these effects by processing the data from an international network of two-frequency receivers of the GPS-GLONASS navigation systems.

7 Acknowledgements

We are grateful to E. A. Ponomarev, V. V. Yevstafiev, A. M. Uralov, P. M. Nagorsky, N. N. Klimov, and A. D. Kalikhman for their interest in this study, helpful advice and active participation in discussions. Authors are grateful to K. S. Palamartchouk and O. S. Lesuta for preparing the input data. Thanks are also due to V. G. Mikhalkosky for his assistance in preparing the English version of the manuscript. This work was done with support from the Russian foundation for Basic Research (grants 97-02-96060 and 99-05-64753), as well as under grant 1999 of the RF Ministry of Education (Minvuz), under direction of B. O. Vugmeister.

References

[1] Afraimovich, E.L., Varshavsky, I.I., Vugmeister, B.O., et al., 1984. Influence of surface industrial explosions on Doppler and angular characteristics of the ionosphere-reflected radio signal. Geomagnetizm i aeronomiya, 24, 322–324 (in Russian).

[2] Afraimovich, E.L., Terechov, A.I., Udodov, M.Yu., and Fridman, S.V., 1992. Refraction distortions of transionospheric radio signals caused by changes in a regular ionosphere and by travelling ionospheric disturbances. Journal of Atmospheric and Solar-Terrestrial Physics, 54, 1013–1020.

[3] Afraimovich, E.L., Palamartchouk, K.S., and Perevalova, N.P., 1998. GPS radio interferometry of travelling ionospheric disturbances. Journal of Atmospheric and Solar-Terrestrial Physics, 60, 1205–1223.

[4] Arendt, P.R., 1971. Ionospheric undulations following 'Appolo–14' launching. Nature, 231, 438–439.

[5] Balachandran, N.K., Donn, W.L., and Kaschak, G., 1971. On the propagation of infrasound from rockets: effects of winds. Journal of the Acoustical Society of America, 50 (2), part 1, 397–404.

[6] Bertel, L., Bertin, F., and Testud, J., 1976. De la mesure du contenu electronique integre appliquee a l'observation des ondes de gravite de moyenne echelle. Journal of Atmospheric and Solar-Terrestrial Physics, 38, 261–270.

[7] Blanc, E., and Jacobson, A.R., 1989. Observation of ionospheric disturbances following a 5-kt chemical explosion. 2. Prolonged anomalies and stratifications in the lower thermosphere after shock passage. Radio Science, 24, 739–746.

[8] Calais, E. and Minster, J.B., 1995. GPS detection of ionospheric perturbations following the January 1994, Northridge earthquake. Geophysical Research Letters, 22, 1045–1048.

[9] Calais, E., and Minster, J.B., 1996. GPS detection of ionospheric perturbations following a Space Shuttle ascent. Geophysical Research Letters, 23, 1897–1900.

[10] Calais, E., Minster, J.B., Hofton, M.A., and Hedlin, M.A.H., 1998a. Ionospheric signature of surface mine blasts from Global Positioning System measurements. Geophysical Journal International, 132, 191–202.

[11] Calais, E., Minster, J.B., and Bernard, J., 1998b. GPS, Earthquake, the ionosphere and Space Shuttle. Physics of Earth and Planet, 105, 167–181.

[12] Davies, K., 1969. Ionospheric radio waves. Blaisdell Publishing Company. A Division of Ginn and Company. Waltham, Massachusetts-Toronto-London.

[13] Fitzgerald, T.J., 1997. Observations of total electron content perturbations on GPS signals caused by a ground level explosion. Journal of Atmospheric and Solar-Terrestrial Physics, 59, 829–834.

[14] Gurtner, W., 1993. RINEX: The Receiver Independent Exchange Format Version 2. http://igscb.jpl.nasa.gov/igscb/data/format/rinex2.txt

[15] Hofmann-Wellenhof, B., Lichtenegger, H., and Collins, J., 1992. Global Positioning System: Theory and Practice, Springer-Verlag Wien, New York.

[16] Jacobson, A.R., Carlos, R.C., and Blanc, E., 1988. Observation of ionospheric disturbances following a 5-kt chemical explosion. 1. Persistent oscillation in the lower thermosphere after shock passage. Radio Science, 23, 820–830.

[17] Jacobson, A.R., and Carlos, R.C., 1994. Observations of acoustic–gravity waves in the thermosphere following Space Shuttle ascents. Journal of Atmospheric and Solar-Terrestrial Physics, 56, 525–528.

[18] Karlov, V.D., Kozlov, S.I., and Tkachev, G.N., 1980. Large-scale disturbances in the ionosphere produced by rocket flight with the operating engine. Kosmicheskiye issledovaniya, 18, 266–277 (in Russian).

[19] Kaschak, G, Donn, W.L., and Fehr, U., 1970. Long-range infrasound from rockets. Journal of the Acoustical Society of America, 48 (1), part 1, 12–20.

[20] Klobuchar, J.A., 1997. Real-time ionospheric science: The new reality. Radio Science, 32, 1943–1952.

[21] Li, Y.Q., Jacobson, A.R., Carlos, R.C., Massey, R.S., Taranenko, Y.N., and Wu, G., 1994. The blast wave of the Shuttle plume at ionospheric heights. Geophysical Research Letters, 21, 2737–2740.

[22] Mendillo, M., 1981. The effects of rocket launches of the ionosphere. Advances in Space Research, 1, 275–290.

[23] Mendillo, M., 1982. Modification of the ionosphere by large space vehicles. Advances of Space Research, 2, 150–159.

[24] Mercier, C. and Jacobson, A.R., 1997. Observations of atmospheric gravity waves by radio interferometry: are results biased by the observational technique? Annales Géophysicae, 15, 430–442.

[25] Nagorsky, P.M., 1998. The inhomogeneous structure of the ionospheric F-region produced by rockets. Geomagnetizm i aeronomiya, 38, 100–106 (in Russian).

[26] Nagorsky, P.M., 1999. Analysis of the HF radio signal response to ionospehric plasma disturbances caused by shock-acoustic waves. Izvestya VUZov Radiofizika, 42, 36–44 (in Russian).

[27] Noble, S.T., 1990. A large-amplitude traveling ionospheric disturbance exited by the Space Shuttle during launch. Journal of Geophysical Research, 95, 19,037–19,044.

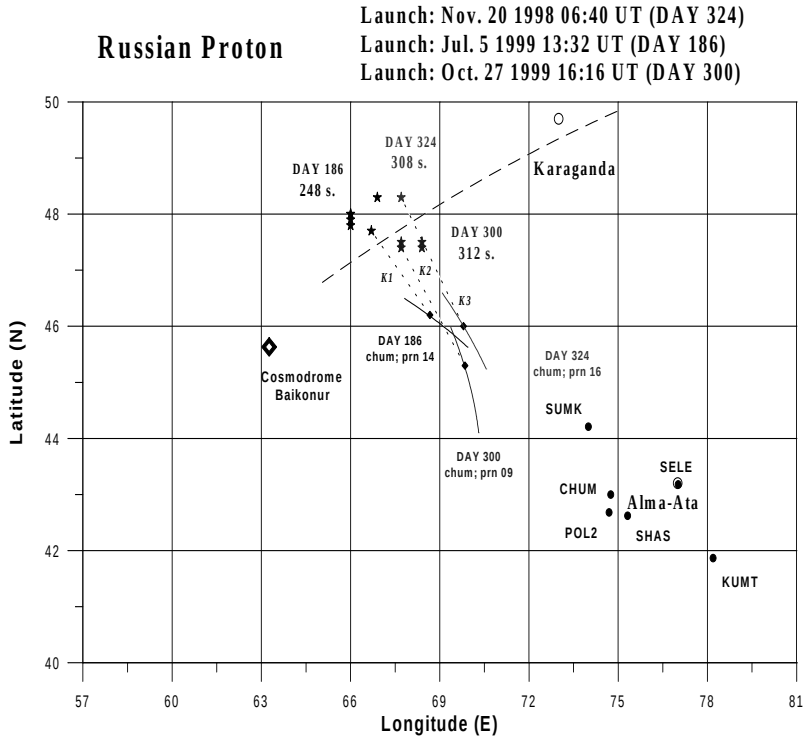

Fig. 1 : Experimental geometry during launches of the Proton launch vehicle from Baikonur Cosmodrome. The dash line roughly corresponds to the horizontal projection of the rocket flight trajectory with orbital inclination 51.6°. The symbol ◇ marks the position of the launch pad. Solid lines show trajectories of subionospheric points for each GPS satellite at the height h_{max} = 400 km. Dark boxies along the trajectories show the position of subionospheric points at the time t_p of a maximum deviation of the frequency Doppler shift F. Asterisks show the source position at 100 km altitude determined using the data from the GPS-arrays. Numbers at the asterisks correspond to day numbers and to the 'switch-on' delay of the source with respect to the start time. Dashed straight lines connecting the anticipated source with the subionospheric point designate the horizontal projection of the wave vector $\boldsymbol{K}$. Heavy dots and upper-case letters mark the position and names of the GPS stations, while lower-case letters along the trajectories refer to station names and PRN numbers of the GPS satellites.

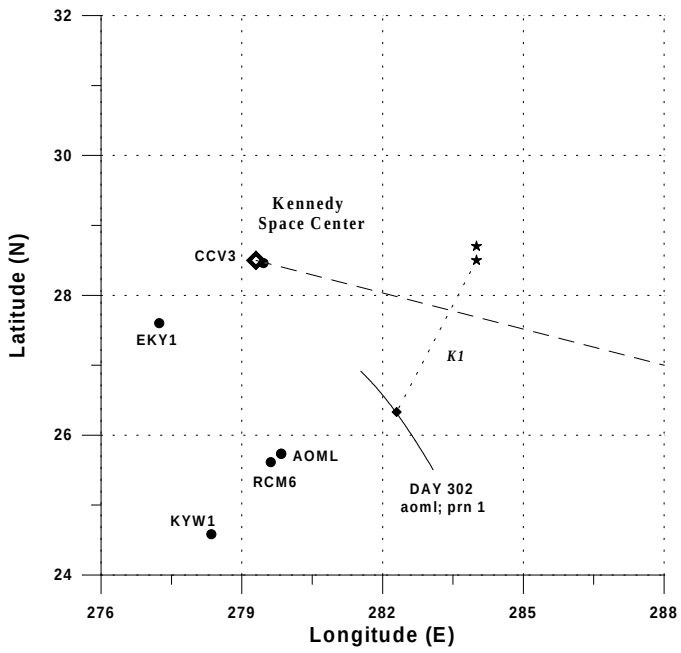

Fig. 2 : Experimental geometry during launches of the Space Shuttle launch vehicle from the Kennedy Space Center Cosmodrome (the designations are the same as in Fig. 1

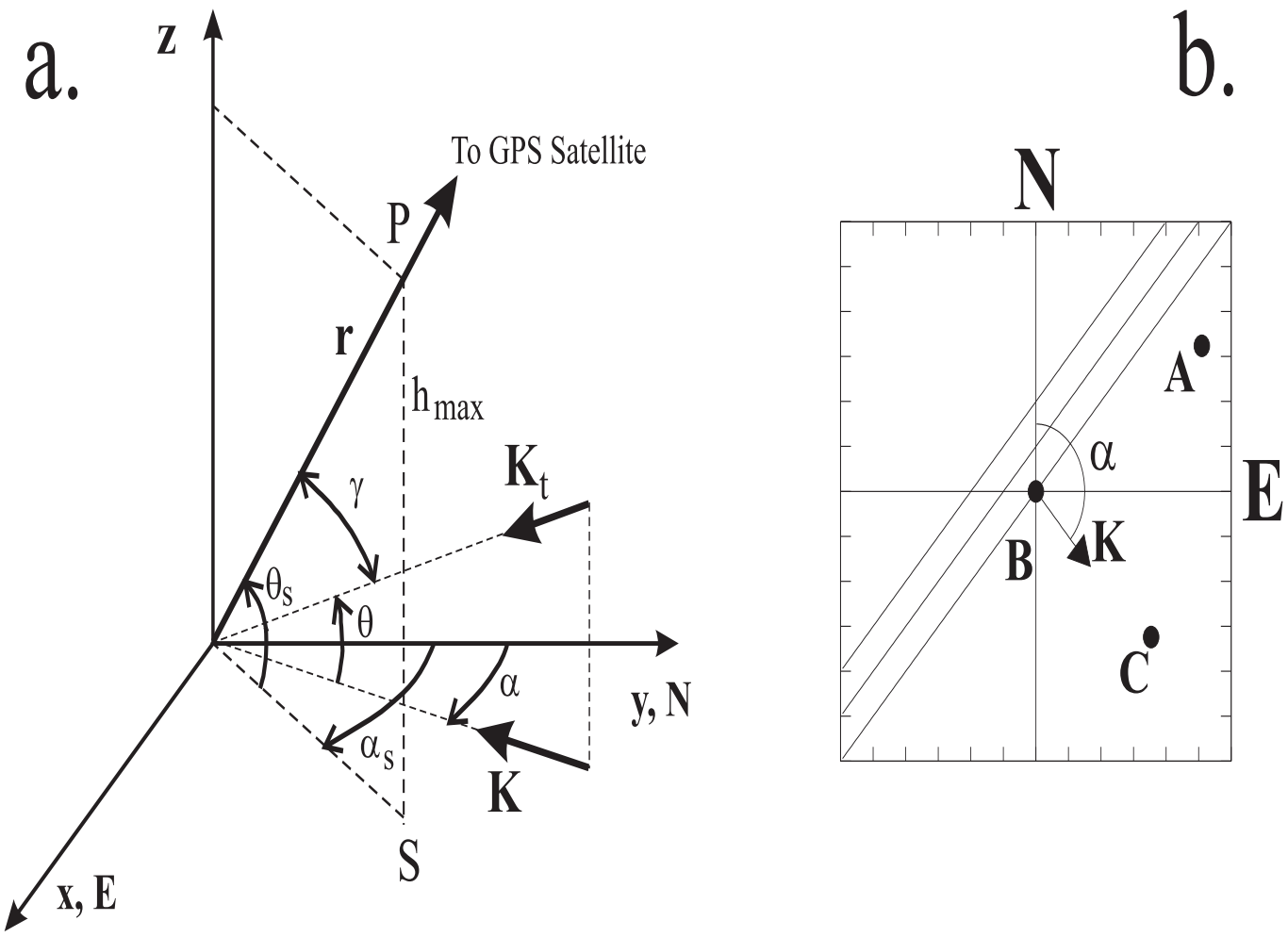

Fig. 3 : **a)** Schematic representation of the transionospheric sounding geometry. The axes z, y, and x are directed, respectively, zenithward, northward (N) and eastward (E). P — point of intersection of Line-of-Sight (LOS) to the satellite with the maximum of the ionospheric $F2$-region; S — subionospheric point; α_s —the azimuthal angle, counted off from the northward in a clockwise direction; and θ_s —the angle of elevation between the direction $\boldsymbol{r}$ along LOS and the terrestrial surface at the reception site. γ — the angle between the vectors $\boldsymbol{K}_t$ and $\boldsymbol{r}$. **b)** GPS-array geometry. A,B,C — receiver poin by about several tens of kilometers, at which two-frequency multichannel GPS-receivers are installed. Parallel lines correspond to lines of equal TEC. The arrow indicates the vector $\boldsymbol{K}$ in the direction α; N, E — northward and eastward directions.

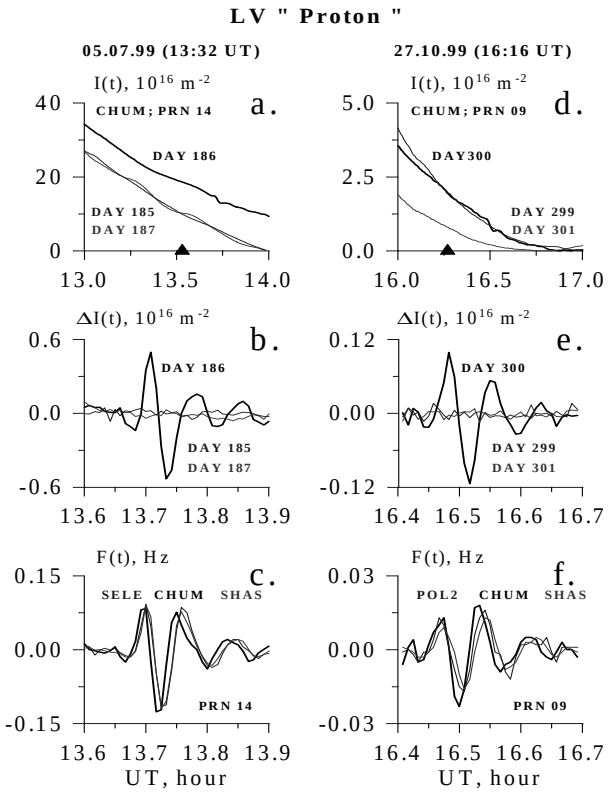

Fig. 4 : Time dependencies of 'oblique' TEC $\Delta I(t)$ at one of the three sites of the GPS-array in the area of Baikonur Cosmodrome on the days of Proton LV launch (heavy curve), and one day before and one day after the start (thin curves) on July 5, 1998 — panel a, and on October 27, 1999 — panel d; panels b, e — for the same days but the TEC variations $\Delta I(t)$ with the linear trend removed and with a smoothing with a time window of 5 min; panels c, f — variations of the frequency Doppler shift $F(t)$ 'reduced' to the sounding signal frequency of 136 MHz, for three sites of the arrays, start days. All panels show day numbers, GPS station names, and PRN numbers of the GPS satellites. The small arrows at the abscissa axis indicate the start time t_0.

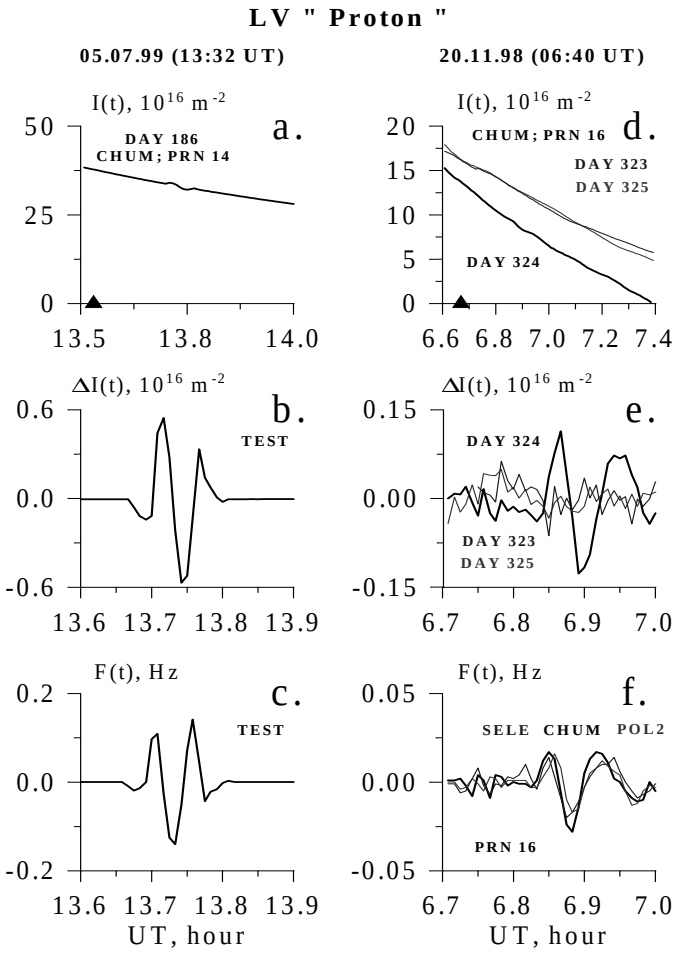

Fig. 5 : Same as in Fig. 4, but in the area of Baikonur Cosmodrome, for Proton LV launch on November 20, 1998 (right). Left — SAW perturbation model for Proton LV launch on July 5, 1999 in the form of a wave packet with a period of 240 s, the packet's duration of 240 s, a maximum amplitude of 0.5 $TECU$, the horizontal phase velocity V_h = 1200 m/s, the azimuth α, and the elevation θ of the wave vector $\boldsymbol{K}_t$ of 153° and 60°, respectively (see Fig. 4 at the left).

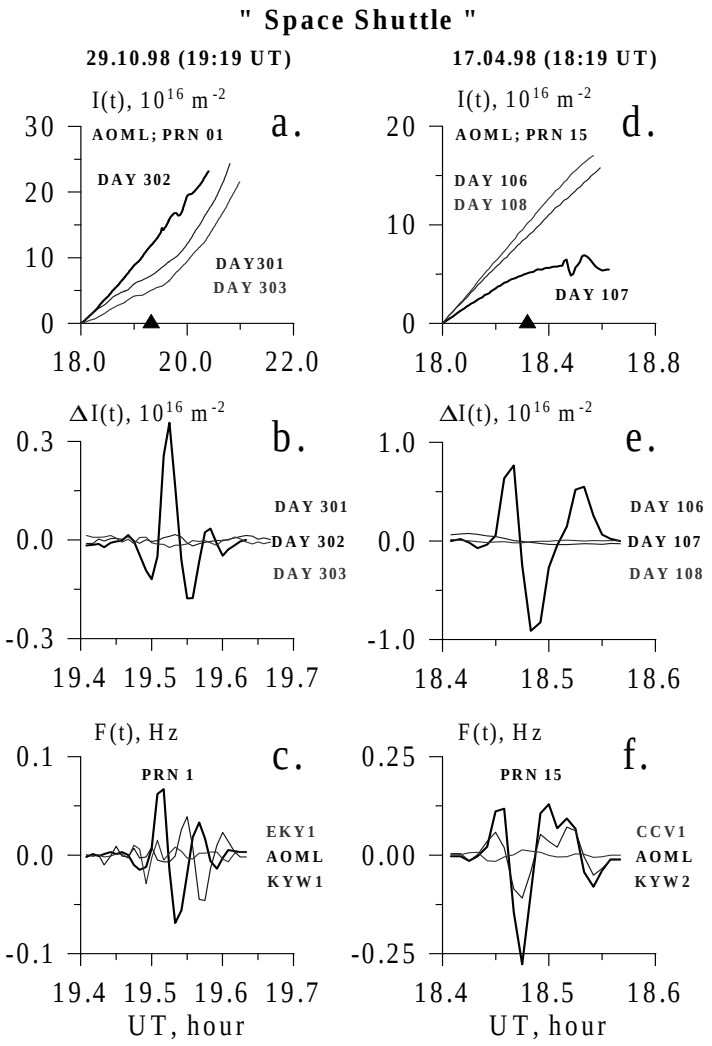

Fig. 6 : Same as in Fig. 4, but in the area of Kennedy Space Center Cosmodrome, for launches of April 17 and October 29, 1998.

Table 1 : GPS site names and locations

N	SITE	Geograph. latitude	Geograph. longitude
Kazakstan			
1	SUMK	44.208	73.997
2	SELE	43.178	77.016
3	CHUM	42.998	74.751
4	POL2	42.679	74.694
5	SHAS	42.620	75.315
6	KUMT	41.864	78.190
Cape Canaveral			
1	CCV3	28.460	279.457
2	CCV1	28.460	279.457
3	EKY1	27.600	277.240
4	AOML	25.735	279.838
5	MIA3	25.732	279.840
6	MIA1	25.733	279.840
7	KYW1	24.582	278.347
8	KYW2	24.582	278.348
9	RCM6	25.614	279.616

Table 2 : Common information about rocket launches

N	Name	Data	t_0 (UT)	t_0 (LT)	ψ (deg)	DST (nT)
1	Proton	Nov. 20 1998 (DAY 324)	06:40	11:40	51.6	-9
2	Proton	Jul. 5 1999 (DAY 186)	13:32	18:32	51.6	11
3	Proton	Oct. 27 1999 (DAY 300)	16:16	21:16	51.6	-80
4	Shuttle	Apr. 17 1998 (DAY 107)	18:19	03:19	39	-37
5	Shuttle	Oct. 29 1998 (DAY 302)	19:19	04:19	28.45	-15

Table 3 : The parameters of Shock-Acoustic Waves for "Proton" launches

No.	Sites	t_p (UT)	Δt, sec.	T, sec.	A_I, TECU	A_F, Hz	ff; °	`; °	V_h, m/s	V_t, m/s	V_α, m/s	'$_w$; ° ˘$_w$; °	Δt_w, sec.
1999 Jul. 5; t_0=13:32 UT													
1	SELE CHUM SHAS	13:44:44	764	300	0.46	0.12	58.9	153	1808	931	1070	48 66	264
2	SUMK POL2 SELE	13:42:44	644	300	0.75	0.17	58	157	1639	874	976	47.9 66	259
3	KUMT SHAS SELE	13:45:54	834	360	0.36	0.08	59	152	2473	1271	1094	47.7 66.7	265
4	POL2 SELE KUMT	13:44:32	752	300	0.39	0.11	58.7	154	2458	1278	894	47.8 66	262
5	CHUM SELE SUMK	13:44:09	729	300	0.49	0.13	58.8	154	1741	901	926	48 66	263
6	$\sum$			305	0.48	0.12	58.7	154	2024	1051	992	47.9 66.1	263
1999 Oct. 27; t_0=16:16 UT													
7	CHUM POL2 SHAS	16:30:58	899	300	0.098	0.02	46.5	161	1679	1156	823	47.5 67.7	308
8	SUMK POL2 SHAS	16:29:31	811	270	0.12	0.038	46.3	162	1666	1151	827	47.4 68.4	325
9	SHAS CHUM SUMK	16:31:31	931	300	0.053	0.016	45.9	163	1659	1155	844	47.5 68.4	302
10	POL2 CHUM SUMK	16:31:18	918	270	0.067	0.017	46.8	161	1666	1151	811	47.4 67.7	312
11	$\sum$			285	0.08	0.02	46.4	162	1668	1153	826	47.5 68	312
1998 Nov. 20; t_0=06:40 UT;													
12	CHUM SELE POL2	6:53:42 6:54:06 6:54:06	822 846 846	300 300 300	0.11 0.09 0.08	0.028 0.02 0.017	52.8	162.9	1338	809	890	48.3 67.7	308

Table 1 : The parameters of Shock-Acoustic Waves for "Space Shuttle" launches

No.	Sites	t_p (UT)	Δt, sec.	T, sec.	A_I, TECU	A_F, Hz	$ff;^\circ$	$`;^\circ$	V_h, m/s	V_t, m/s	V_α, m/s	$'_w;^\circ$ $\breve{}_w;^\circ$	Δt_w, sec.
1998 Oct. 29; t_0=19:19 UT													
1	AOML KYW1 EKY1	19:30:47 19:32:54 19:30:29	707 834 689	210 210 240	0.36 0.2 0.06	0.069 0.048 0.029	34.7	214	1502	1236	798 694 592	28.5 284	204
2	MIA3 KYW1 EKY1	19:30:52	712	210	0.44	0.086	34	213	1556	1290	852	28.7 284	202
3	$\sum$			218	0.27	0.05	34.4	213.5	1529	1263	734	28.6 284	203
1998 Apr. 17; t_0=18:19 UT													
4	CCV1 RCM6 KYW2	18:27:59 18:29:09 18:29:12	539 609 612	270 270 240	0.38 0.55 0.50	0.1 0.13 0.13	31.6	141	3640	3101	1524 1207 1060	36.8 284	–
5	AOML CCV1 KYW2	18:29:11	611	270	0.76	0.27	29.3	139	3540	3086	1231	37 284	–
6	$\sum$			263	0.57	0.16	30.5	140	3590	3094	1255	36.9 284	–